Black-bounce solution in *k*-essence theories

Carlos F. S. Pereira[*]
Departamento de Física, Universidade Federal do Espírito Santo, Avenida Fernando Ferrari, 514, Goiabeiras, 29060-900, Vitória, Espírito Santo, Brazil

Denis C. Rodrigues[†]
Núcleo Cosmo-ufes and Departamento de Física, Universidade Federal do Espírito Santo, Avenida Fernando Ferrari, 514, Goiabeiras, 29060-900, Vitória, Espírito Santo, Brazil

Júlio C. Fabris[‡]
Núcleo Cosmo-ufes and Departamento de Física, Universidade Federal do Espírito Santo, Avenida Fernando Ferrari, 514, Goiabeiras, 29060-900, Vitória, Espírito Santo, Brazil and National Research Nuclear University MEPhI (Moscow Engineering Physics Institute), 115409, Kashirskoe shosse 31, Moscow, Russia

Manuel E. Rodrigues[§]
Faculdade de Ciências Exatas e Tecnologia, Universidade Federal do Pará Campus Universitário de Abaetetuba, 68440-000, Abaetetuba, Pará, Brazil and Faculdade de Física, Programa de Pós-Graduação em Física, Universidade Federal do Pará, 66075-110, Belém, Pará, Brazil

(Received 30 September 2023; accepted 8 January 2024; published 5 February 2024)

In the present work, we construct black-bounce configurations in the context of *k*-essence theory. The solutions have a regular metric function at the origin. The area metric function is linked to the black-bounce area initially considered by Simpson-Visser, $\Sigma^2 = x^2 + a^2$. Subsequently, the expressions for the scalar field and scalar potential corresponding to the found solutions are determined, exhibiting phantom behavior everywhere due to violation of the null energy condition (NEC^{ϕ}). The Kretschmann scalar is regular in spacetime, and the geodesics are complete. The energy conditions are analyzed, verifying that the null (NEC_1^{ϕ}) and dominant energy conditions (DEC_1^{ϕ}) are violated inside and outside the event horizon. Finally, the extrinsic curvature method is applied to determine the sign of the mass on the junction surface.

DOI: 10.1103/PhysRevD.109.044011

I. INTRODUCTION

Recently, Simpson and Visser [1] introduced a new class of solutions called "black-bounce" describing regular black holes and traversable wormholes. These solutions have a nonzero throat radius $a^2 \neq 0$ and reduce to the Schwarzschild metric when $a \to 0$. Subsequent studies have explored generalizations and applications of the black-bounce solutions. Lobo *et al.* [2] constructed new black-bounce solutions by modifying the mass function, recovering the original Simpson-Visser solution [1] for particular parameter values. Rodrigues and Silva [3] investigated the Simpson-Visser black-bounce geometry with modifications to the metric function related to the black-bounce area. Junior and Rodrigues [4] obtained novel black-bounce solutions in the context of $f(T)$ modified gravity theory.

The search for exotic solutions such as regular black holes and traversable wormholes requires violating standard energy conditions: the minimally coupled canonical scalar field cannot describe such geometries. However, Bronnikov and Fabris showed a canonical scalar field with phantom behavior can allow regular black holes [5]. In this context, *k*-essence theory has emerged as an exotic matter alternative, with its noncanonical kinetic term displaying phantom behavior without exotic matter. The *k*-essence theories generalize the scalar field kinetic term, originally proposed for modeling primordial inflation with just a kinetic term [6–8]. Generalized kinetic terms are also motivated by string theory [9]. This work examines black-bounce solutions in *k*-essence theory with a power law kinetic term and potential, focusing on energy condition violations.

[*]carlos.f.pereira@edu.ufes.br
[†]deniscr@gmail.com
[‡]julio.fabris@cosmo-ufes.org
[§]esialg@gmail.com

In the studies of static, spherically symmetric configurations, exotic matter is frequently introduced in order to find regular black holes and wormholes solutions in nonlinear electrodynamics. These new regular metrics constitute exact solutions in general relativity, derived through a combined stress-energy tensor of a scalar field with nonzero self-interaction potential and a magnetic field [10–14]. However, rotating metrics have also been found to accommodate such regular objects [15–17]. This analysis investigates black-bounce solutions in k-essence theory to gain insights into k-essence and exotic solutions in general relativity.

Furthermore, Bronnikov *et al.* investigated Ellis-Bronnikov wormhole solutions within the framework of extended gravity theories [18]. The analysis reveals that the same wormhole metric arises in both Rastall gravity and k-essence theories, although with distinct stability characteristics. Perturbation analysis exposes inconsistencies in Rastall gravity, whereas the k-essence solution proves to be unstable for specific model parameters. These findings underscore the difficulties encountered in discovering straightforward, traversable, and perturbatively stable wormhole solutions devoid of exotic matter.

The Simpson-Visser metric has been studied in other contexts, such as light deflection and gravitational lensing effects [19–22]. Gravitational lensing was analyzed using black-bounce solutions in a spherically symmetric and stationary spacetime [23,24]. In the zero mass limit, this reduces to the Ellis-Bronnikov charged wormhole. Quantum dynamics have been studied using the Ellis-Bronnikov metric [25–28].

Phantom scalar fields are often studied as a source of exotic matter required to obtain wormhole solutions minimally coupled to general relativity [14,29]. Their phantom properties are typically associated with the violation of energy conditions and occasionally lead to instabilities [30,31]. Additionally, ghost fields are commonly associated with dark energy candidates, further emphasizing the importance of investigations in this direction [32,33]. From this perspective, phantom fields have been explored as a matter source for singular [34,35] and regular black holes [5,36,37].

The present study first establishes in Sec. II the theoretical background of the k-essence model, including the key relationships and equations. Section III then derives the specific metric function corresponding to a defined black-bounce throat geometry, and determines the associated scalar field and potential solutions that satisfy the equations of motion. Next, Sec. IV examines the geometric properties by defining the regular Kretschmann scalar and stress-energy tensor components inside and outside the horizon, as well as analyzing the energy conditions required for the black-bounce solutions. Finally, Sec. V summarizes the main conclusions from this analysis regarding the viability of constructing regular black-bounce geometries within k-essence theories.

II. GENERAL RELATIONS

The k-essence theories are characterized by a noncanonical kinetic term for the scalar field, represented by the Lagrangian

$$\mathcal{L} = \sqrt{-g}[R - F(X,\phi)], \tag{1}$$

where R is the Ricci scalar and $X = \eta\phi_{;\rho}\phi^{;\rho}$ denotes the kinetic term. While k-essence models can include a potential term and nontrivial couplings, the scalar sector is generally minimally coupled to gravity. The parameter $\eta = \pm 1$ avoids imaginary terms in the kinetic expression X. By choosing different forms of the function $F(X,\phi)$, k-essence theories can describe both phantom and standard scalar fields.

The variation of the Lagrangian (1) with respect to the metric and the scalar field yields the field equations:

$$G^{\nu}_{\mu} = -T^{\nu}_{\mu}(\phi) = -\eta F_X \phi_\mu \phi^\nu + \frac{1}{2}\delta^{\nu}_{\mu} F, \tag{2}$$

$$\eta \nabla_\alpha (F_X \phi^\alpha) - \frac{1}{2} F_\phi = 0, \tag{3}$$

where G^{ν}_{μ} is the Einstein tensor, T^{ν}_{μ} the stress-energy tensor, $F_X = \frac{\partial F}{\partial X}$, $F_\phi = \frac{\partial F}{\partial \phi}$, and $\phi_\mu = \partial_\mu \phi$.

The line element representing the most general spherically symmetric and static spacetime takes the form

$$ds^2 = e^{2\gamma(u)}dt^2 - e^{2\alpha(u)}du^2 - e^{2\beta(u)}d\Omega^2, \tag{4}$$

where u is an arbitrary radial coordinate, $d\Omega^2 = d\theta^2 + \sin^2\theta d\varphi^2$ the volume element, and $\phi = \phi(u)$.

The nonzero components of the stress-energy tensor are

$$T^0_0 = T^2_2 = T^3_3 = -\frac{F}{2}, \tag{5}$$

$$T^1_1 = -\frac{F}{2} - \eta F_X e^{-2\alpha}\phi'^2, \tag{6}$$

with $\phi' = \frac{d\phi}{du}$.

It is assumed that the function $X = -\eta e^{-2\alpha}\phi'^2$ is positive, which implies that $\eta = -1$. As a result, the equations of motion take the form

$$2(F_X e^{-\alpha+2\beta+\gamma}\phi')' - e^{\alpha+2\beta+\gamma}F_\phi = 0, \tag{7}$$

$$\gamma'' + \gamma'(2\beta' + \gamma' - \alpha') - \frac{e^{2\alpha}}{2}(F - XF_X) = 0, \tag{8}$$

$$-e^{2\alpha-2\beta} + \beta'' + \beta'(2\beta' + \gamma' - \alpha') - \frac{e^{2\alpha}}{2}(F - XF_X) = 0, \tag{9}$$

$$-e^{-2\beta}+e^{-2\alpha}\beta'(\beta'+2\gamma')-\frac{F}{2}+XF_X=0. \quad (10)$$

The notation used here follows the same as used in Ref. [38]. The following coordinate transformation is defined: $u=:x$, and the *quasiglobal* gauge $\alpha(u)+\gamma(u)=0$ is employed. As a result, the line element in Eq. (4) can be expressed in the following form:

$$ds^2=A(x)dt^2-\frac{dx^2}{A(x)}-\Sigma^2(x)d\Omega^2, \quad (11)$$

where the metric functions are defined as $A(x)=e^{2\gamma}=e^{-2\alpha}$ and $e^{\beta}=\Sigma(x)$. The equations of motion defined in Eqs. (7)–(10) can then be rewritten in the new coordinates. Combining Eqs. (8)–(10) yields the expressions

$$2A\frac{\Sigma''}{\Sigma}-XF_X=0, \quad (12)$$

$$A''\Sigma^2-A(\Sigma^2)''+2=0, \quad (13)$$

where the primes now represent derivatives with respect to x.

The two remaining equations, Eqs. (7) and (10), are rewritten in the new coordinates as

$$2(F_X A\Sigma^2\phi')'-\Sigma^2F_\phi=0, \quad (14)$$

$$\frac{1}{\Sigma^2}(-1+A'\Sigma'\Sigma+A\Sigma'^2)-\frac{F}{2}+XF_X=0. \quad (15)$$

For the remainder of this analysis, the k-essence function is defined as $F(X)=F_0X^n-2V(\phi)$, where F_0 is a constant parameter, n is a real number, $X=\eta\phi_{;\rho}\phi^{;\rho}$ is the kinetic term, and $V(\phi)$ represents the potential.

III. GENERAL SOLUTION

The analysis aims to find black-bounce solutions to the k-essence equations of motion [1,39]. The metric function $\Sigma^2(x)=x^2+a^2$ from the original work [1] is used, where the nonzero throat radius a gives regular black holes or wormholes, with the area function $\Sigma^2(x)$ and the k-essence equations of motion, Eq. (13), the corresponding metric function $A(x)$ is derived.

The general solution of the differential equation (13) is given by

$$A(x)=1+C_1\left[(x^2+a^2)\arctan\left(\frac{x}{a}\right)+xa\right]+C_2(x^2+a^2), \quad (16)$$

where C_1 and C_2 are constants.

Certain requirements were imposed on the solution Eq. (16), such as being asymptotically flat, leading to a constraint between the constants $C_2=-\frac{\pi}{2}C_1$. Furthermore, the solution should approach the Simpson-Visser solution as $x\to 0$, namely, $A(x\to 0)=1-\frac{2m}{a}$. Hence, the constant is set as $C_1=\frac{4m}{\pi a^3}$. The resulting solution is

$$A(x)=1+\left(\frac{4m}{\pi a^3}\right)\left[xa+(x^2+a^2)\left(\arctan\left(\frac{x}{a}\right)-\frac{\pi}{2}\right)\right]. \quad (17)$$

Figure 1(a) shows curves of the metric function from Eq. (17) for various throat radii a, inside and outside the event horizon. For all a, $A(x)$ diverges as $x\to-\infty$ and is asymptotically flat as $x\to\infty$. This general solution of Eq. (17) is regular at the origin and for $x\to-\infty$, asymptotically approaching to de Sitter–Schwarzschild form. This requires considering the series expansion of $\arctan(\frac{x}{a})$ for $x\to-\infty$ and discarding higher order terms $\mathcal{O}(\frac{1}{x})$.

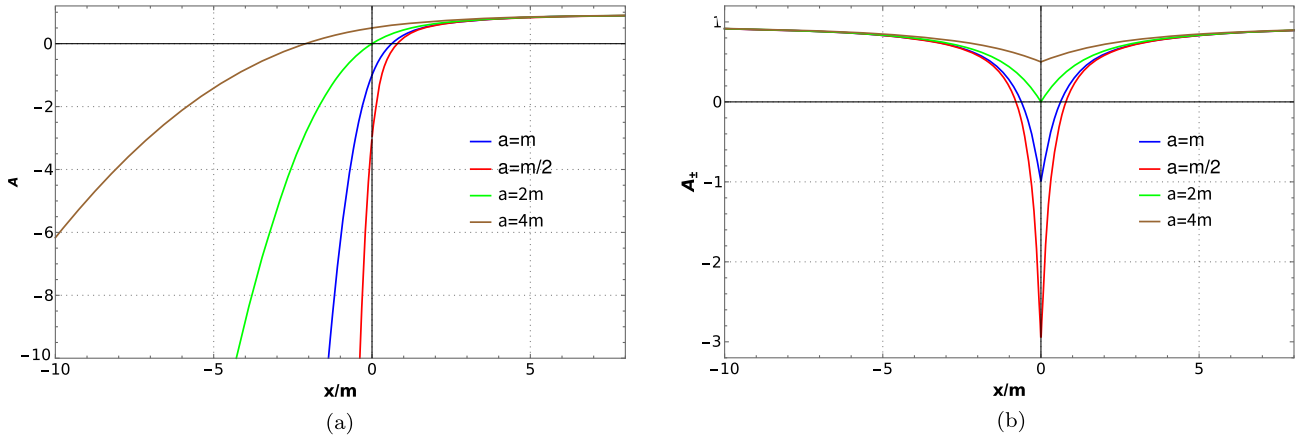

(a) (b)

FIG. 1. (a) Curves for various throat radius values a; the function is not asymptotically flat in both $x\to\pm\infty$ limits. (b) Radii inside and outside the horizon, with the metric function defined by matching asymptotically flat solutions at $x=0$ for $x\to\pm\infty$.

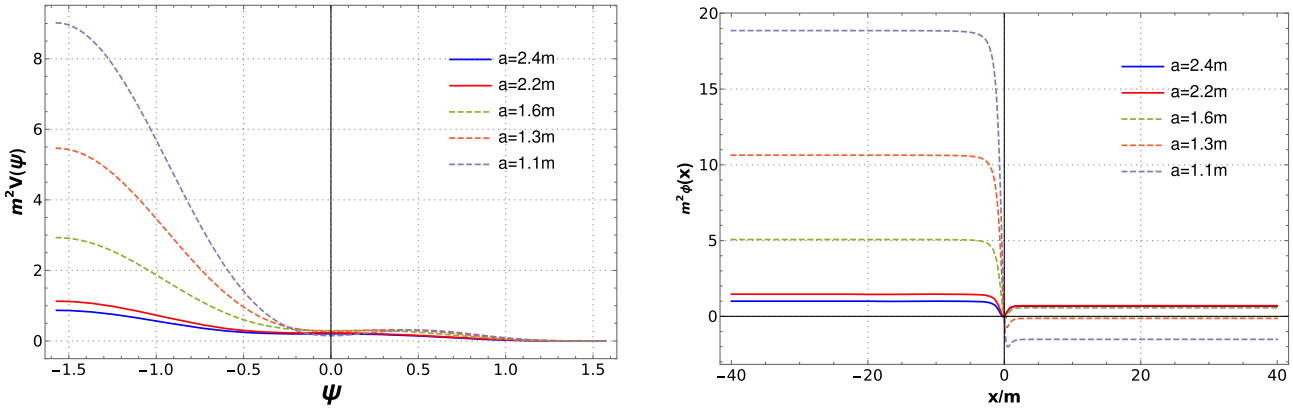

(a) (b)

FIG. 2. Graphing for the scalar field and potential for the general metric function Eq. (17) with radius values of throats outside the inside event horizon. We fixed the constant $F_0 = 1$.

Taking the general metric function in Eq. (17) gives

$$A(x) = 1 - \frac{8m}{3\pi}\left(\frac{1}{x}\right) - \frac{4m}{a^3}(x^2 + a^2). \tag{18}$$

The general metric function in Eq. (17) is equivalent to the solution in Eq. (10) from [5], with redefinitions $\rho_0 = \frac{4m}{\pi}$ and $c = -\frac{2m}{a}$. This corresponds to the canonical $n = 1$ phantom scalar field case in k-essence theory. The regularity of the general solution in Eq. (17) can be seen in the Kretschmann scalar in Fig. 6(a), which tends to zero as $x \to \infty$ (Minkowski limit) and is constant and positive as $x \to -\infty$.

The behavior of the scalar field for the obtained k-essence solution, with $n = \frac{1}{3}$, can be examined using the general metric solution in Eq. (17). The scalar field $\phi(x)$ for this metric is given by

$$\begin{aligned}\phi(x) = {} & \frac{D_1}{4a^5}\left[\frac{xa^3}{\Sigma^4} + \frac{3xa}{2\Sigma^2} + \frac{3}{2}\arctan\left(\frac{x}{a}\right)\right] \\ & - \frac{D_1 m}{\pi a^2 \Sigma^4} - \frac{D_1 m}{a^6}\left[\frac{ax}{\Sigma^2} + \arctan\left(\frac{x}{a}\right)\right] \\ & + \left(\frac{2D_1 m}{\pi a^6}\right)\left[\frac{a^2}{2\Sigma^2} + \arctan\left(\frac{x}{a}\right)\right. \\ & \left. \times \left(\frac{xa}{\Sigma^2} + \frac{1}{2}\arctan\left(\frac{x}{a}\right)\right)\right],\end{aligned} \tag{19}$$

where $D_1 = (\frac{6a^2}{F_0})^{\frac{3}{2}}$ is a constant.

As shown in Fig. 2(b), $\phi(x)$ approaches constant values depending on the throat radius a as $x \to \pm\infty$, specifically

$$\phi(x \to -\infty) = -\frac{9\pi\sqrt{\frac{3}{2}}}{4a^3}(a - 4m) \quad \text{and}$$
$$\phi(x \to \infty) = \frac{3\pi\sqrt{\frac{3}{2}}}{4a^3}(3a - 4m), \tag{20}$$

where we set $F_0 = 1$.

Similarly, the potential $V(\phi(x))$ can be analyzed. The potential for the metric in Eq. (17) is given by

$$\begin{aligned}V(\phi(x)) = {} & \frac{2a^2}{\Sigma^4} - \frac{cax}{\Sigma^4}(\Sigma^2 + 2x^2) \\ & - \frac{c}{\Sigma^2}(3x^2 - a^2)\left[\arctan\left(\frac{x}{a}\right) - \frac{\pi}{2}\right],\end{aligned} \tag{21}$$

where $c = \frac{4m}{\pi a^3}$ is a combination of constants.

To better represent the potential, the transformation $\psi = \arctan(\frac{x}{a})$ is performed, and the potential is rewritten in terms of this new variable ψ. Thus, in asymptotic analysis, taking the limit $x \to \pm\infty$ is equivalent to taking $\psi \to \pm\frac{\pi}{2}$. The potential is therefore expressed as

$$\begin{aligned}V(\psi) = {} & \frac{2\cos^4(\psi)}{a^2} + \frac{c\sin(2\psi)}{2}[\cos(2\psi) - 2] \\ & + c\left(\psi - \frac{\pi}{2}\right)[2\cos(2\psi) - 1].\end{aligned} \tag{22}$$

As Fig. 2 exhibits, $V(\psi)$ tends to the constant $3\pi c$ as $x \to -\infty$ and to zero as $x \to \infty$.

A. Black-bounce solution

In order to construct black-bounce solutions, the general solution in Eq. (17) will be matched to construct the appropriate geometry.

First, the requirement was imposed that the metric function be asymptotically flat in both limits, to recover

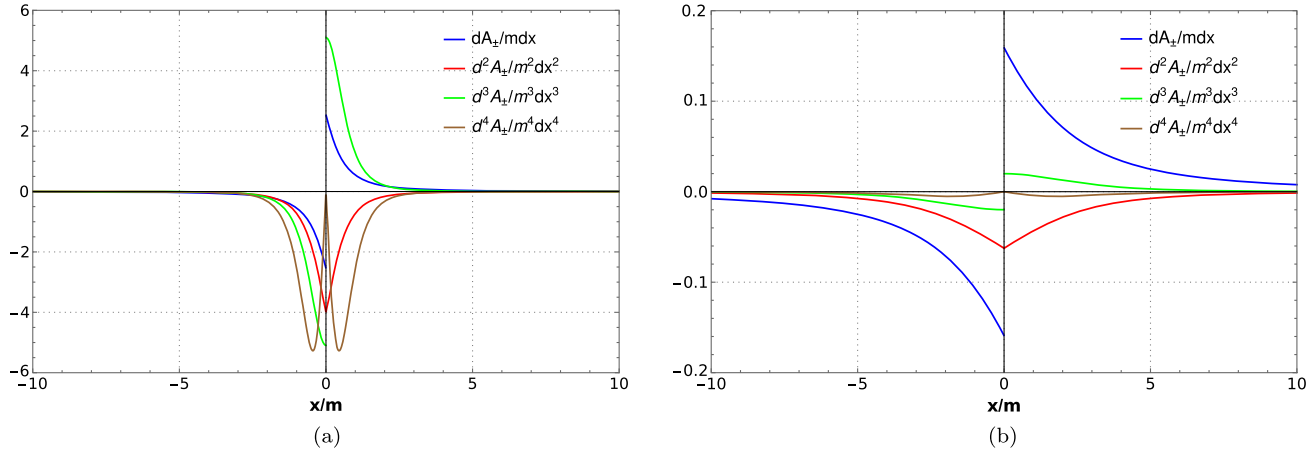

FIG. 3. (a) The odd and even derivatives of the asymptotically flat function Eq. (23) for a radius $a = m$ inside the horizon. (b) The derivatives for a radius $a = 4m$ outside the horizon.

the Schwarzschild metric. To achieve this, the metric function Eq. (17) was bisected at $x = 0$ and mirrored, defining two regions [see Fig. 1(b)]. The metric function is thus expressed as

$$A_+(x) = 1 + \left(\frac{4m}{\pi a^3}\right)\left[xa + (x^2 + a^2)\left(\arctan\left(\frac{x}{a}\right) - \frac{\pi}{2}\right)\right], \quad x \geq 0,$$
$$A_-(x) = 1 - \left(\frac{4m}{\pi a^3}\right)\left[xa + (x^2 + a^2)\left(\arctan\left(\frac{x}{a}\right) + \frac{\pi}{2}\right)\right], \quad x \leq 0. \tag{23}$$

Figure 3 shows curves of derivatives up to fourth order for the metric function Eq. (23). Figure 3(a) shows the derivatives for a throat radius $a = m$ inside the event horizon. Figure 3(b) displays the derivatives for a radius $a = 4m$ outside the event horizon.

The odd derivatives of the metric function Eq. (23) exhibit discontinuity at the origin, as shown in Fig. 3, while even derivatives are continuous, as expected for a smooth function. This arises due to the construction method in Eq. (23) and implies a spherically symmetric thin shell exists at the junction point $x = 0$. Consequently, black-bounce solutions are obtained only for the cases of the wormhole traversable in both directions $a > 2m$ and the wormhole with two horizons $a < 2m$. The possibility of one-way traversable wormholes with $a = 2m$ is ruled out. This restriction is further examined in the Appendix and is similar to previous studies [4].

In order to enhance the depiction of graphs throughout the study, it will be advantageous to utilize the variable transformation $y = \frac{x}{a}$, enabling the expression of physical quantities in terms of the mass m.

At this stage, the metric functions have been constructed to meet all necessary conditions. The set of equations of motion, Eqs. (12)–(15), can be rewritten in terms of the metric function $A_\pm(x)$ for each region.

Equation (13) was used for the area metric function from the original work [1] to derive the corresponding function $A_\pm(x)$. To obtain the associated scalar field, Eq. (12) is solved for the k-essence field, defined as $X = -\eta A_\pm \phi'^2$ and $F(X) = F_0 X^n - 2V(\phi)$, where F_0 is a constant, n is real, and $V(\phi)$ is the potential. With fixed $n = \frac{1}{3}$ and $\eta = -1$, Eq. (12) becomes

$$\phi'_\pm = \left(\frac{6}{F_0}\frac{\Sigma''}{\Sigma}\right)^{\frac{3}{2}} A_\pm. \tag{24}$$

The above relation is a first order differential equation containing only the metric functions Σ and $A_\pm$. Direct integration produces the scalar field $\phi_\pm(x)$, already found in Eq. (19), now, for each region

$$\phi_\pm(x) = \frac{D_1}{4a^5}\left[\frac{xa^3}{\Sigma^4} + \frac{3xa}{2\Sigma^2} + \frac{3}{2}\arctan\left(\frac{x}{a}\right)\right] \mp \frac{D_1 m}{\pi a^2 \Sigma^4} - \frac{D_1 m}{a^6}\left[\frac{ax}{\Sigma^2} + \arctan\left(\frac{x}{a}\right)\right] \pm \left(\frac{2D_1 m}{\pi a^6}\right)\left[\frac{a^2}{2\Sigma^2} + \arctan\left(\frac{x}{a}\right) \times \left(\frac{xa}{\Sigma^2} + \frac{1}{2}\arctan\left(\frac{x}{a}\right)\right)\right], \tag{25}$$

where

$$\phi(x) = \begin{cases} \phi_+, & x \geq 0, \\ \phi_-, & x \leq 0, \end{cases} \tag{26}$$

where $D_1 = \left(\frac{6a^2}{F_0}\right)^{\frac{3}{2}}$ is a constant. Hence, the scalar field described by Eq. (25) reaches its maximum value as $\phi_+(x \to \infty)$ and its minimum value as $\phi_-(x \to -\infty)$.

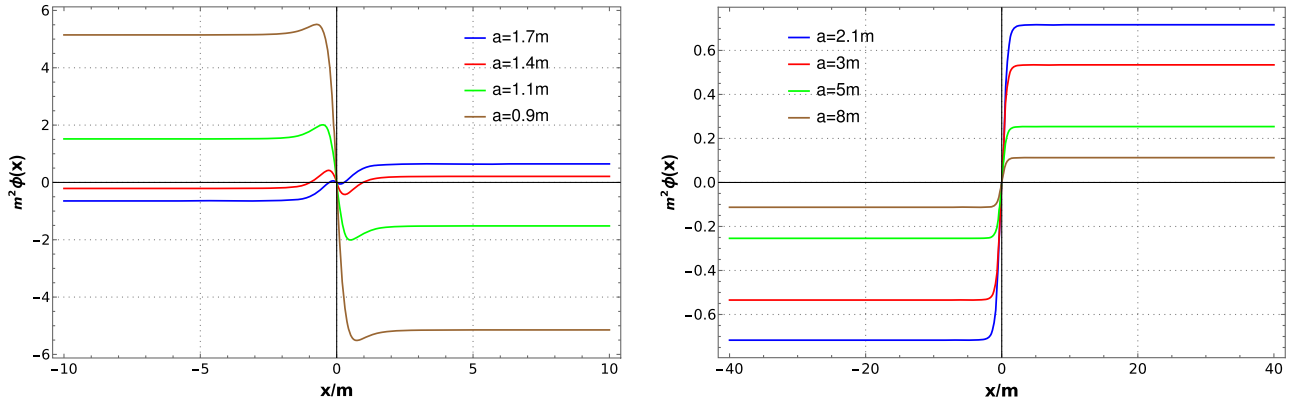

FIG. 4. Curves of the scalar field equation (25) for throat radii inside the horizon are displayed in (a), with constant $F_0 = 1$. In (b), curves are exhibited for radii outside the horizon, also fixing $F_0 = 1$.

The corresponding expressions for these values are defined below:

$$\phi_{\max} = \phi_+(x \to \infty) = \frac{3\pi\sqrt{\frac{3}{2}}}{4a^3}(3a - 4m) \quad \text{and}$$
$$\phi_{\min} = \phi_-(x \to -\infty) = -\frac{9\pi\sqrt{\frac{3}{2}}}{4a^3}(a - 4m), \tag{27}$$

where we set $F_0 = 1$.

To satisfy the system Eqs. (12)–(15), a scalar potential is required. Equation (15) is thus used together with the metric functions Σ and $A_\pm(x)$ and the scalar field equation (25) to define the associated potential $V_\pm(\phi(x))$:

$$V_\pm(\phi(x)) = A_\pm\frac{\Sigma''}{\Sigma} + \frac{1}{\Sigma^2} - \frac{A'_\pm\Sigma'}{\Sigma} - \frac{A_\pm\Sigma'^2}{\Sigma^2}. \tag{28}$$

The potential in Eq. (28) is obtained through a procedure analogous to the scalar field definition in Eq. (25). With some algebraic simplifications, it can be expressed explicitly as

$$V_\pm(\phi(x)) = \frac{2a^2}{\Sigma^4} \mp \frac{cax}{\Sigma^4}(\Sigma^2 + 2x^2) \mp \frac{c}{\Sigma^2}(3x^2 - a^2)\left[\arctan\left(\frac{x}{a}\right) \mp \frac{\pi}{2}\right], \tag{29}$$

where

$$V(\phi(x)) = \begin{cases} V_+, & x \geq 0, \\ V_-, & x \leq 0, \end{cases} \tag{30}$$

where $c = \frac{4m}{\pi a^3}$ is a combination of constants. The potential equation (30) approaches zero as $x \to \pm\infty$, and near the origin, it tends toward $\frac{2(a-m)}{a^3}$.

As in the previous section, to better represent the potential, the transformation $\psi = \arctan(\frac{x}{a})$ is performed and the potential is rewritten in terms of this new variable ψ. The potential is therefore expressed as

$$V_\pm(\psi) = \frac{2\cos^4(\psi)}{a^2} \pm \frac{c\sin(2\psi)}{2}[\cos(2\psi) - 2] \pm c\left(\psi \mp \frac{\pi}{2}\right)[2\cos(2\psi) - 1]. \tag{31}$$

With the scalar potential defined, verification shows all equations of motion are satisfied. In particular, Eq. (14), which was not used in the derivation, is also satisfied in both regions:

$$\frac{dV_\pm}{dx} + \frac{F_0}{3}\left(\frac{\phi'_\pm}{\Sigma^2}\right)\left(\sqrt{\frac{F_0\Sigma^5}{6\Sigma''}}\right)' = 0. \tag{32}$$

Figures 4 and 5 show the scalar field equation (25) and potential equation (31) for various throat radii. The discontinuity and symmetry in the curves reflects the match procedure for the metric function $A_\pm(x)$. Discontinuities in odd derivatives are also shown.

The scalar field displays oscillations due to its interaction with the thin shell at $x = 0$ for radii values inside the horizon, as depicted in Fig. 4(a). Conversely, the potential functions have a barrier that increases for radii near the event horizon and decreases as the radius value moves away from the horizon, as illustrated in Fig. 5(b). When considering increasingly internal values, the potential exhibits similarities to the Pöschl-Teller potential [40–43] for the radius within the event horizon, as seen in Fig. 5(a).

These characteristics of the potential can be further visualized through the construction of a parametrized graph of the potential equation (30) as a function of the scalar field equation (26). This is exemplified by the curves

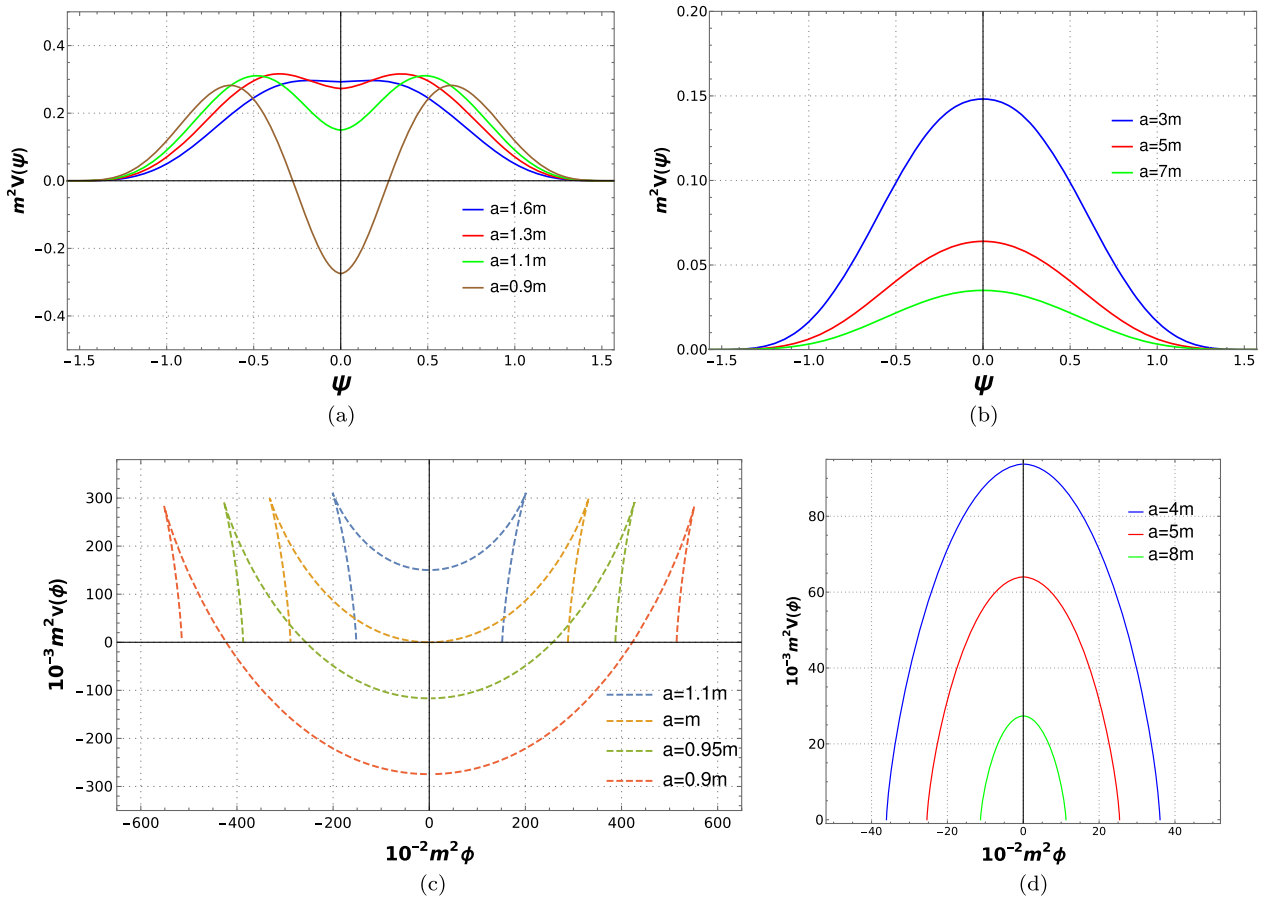

FIG. 5. Curves of the potential equation (31) for throat radii inside the horizon are depicted in (a). In (b), curves are shown for radii outside the horizon. In the remaining panels (c) and (d), we respectively present the behavior of the potential equation (30) as a function of the scalar field equation (26) for selected values of throat radii inside and outside the horizon. Here, we have set $F_0 = 1$.

depicted inside the event horizon, as shown in Fig. 5(c), and outside the event horizon, as illustrated in Fig. 5(d).

Continuing with the parametric graph depicting curves with throat radii within the event horizon, it is evident from Fig. 5(c) that the scalar field attains maximum and minimum values in accordance with the expression provided by its asymptotic Eq. (27). Notably, in this figure, it is apparent that the minimum point of the potential gradually shifts toward the negative side as the radii values move further internally toward the horizon.

IV. GEOMETRIC QUANTITIES

With the solutions constructed, the focus now turns to investigating the geometric properties before analyzing the energy conditions. The spherically symmetric line element is defined as

$$ds^2 = A_{\pm}(x)dt^2 - \frac{dx^2}{A_{\pm}(x)} - \Sigma^2(x)d\Omega^2. \tag{33}$$

Constructing the Kretschmann scalar requires the nonzero Riemann tensor components. With the area metric function defined as $\Sigma^2(x) = x^2 + a^2$, the nonvanishing elements are

$$R^{tr}{}_{tr} = \frac{A''_{\pm}}{2}, \quad R^{\theta\phi}{}_{\theta\phi} = \frac{A_{\pm}\Sigma'^2 - 1}{\Sigma^2},$$
$$R^{t\theta}{}_{t\theta} = R^{t\phi}{}_{t\phi} = \frac{A'_{\pm}\Sigma'}{2\Sigma}, \quad R^{r\theta}{}_{r\theta} = R^{r\phi}{}_{r\phi} = \frac{A'_{\pm}\Sigma' + 2A_{\pm}\Sigma''}{2\Sigma}. \tag{34}$$

Using the nonzero Riemann tensor components from Eq. (34), the Kretschmann scalar $K = R_{\alpha\beta\mu\nu}R^{\alpha\beta\mu\nu}$ can be constructed in terms of the Riemann tensor as a semipositive sum of quadratic terms [2,44]:

$$K = 4(R^{tr}{}_{tr})^2 + 4(R^{t\theta}{}_{t\theta})^2 + 4(R^{t\phi}{}_{t\phi})^2 + 4(R^{r\theta}{}_{r\theta})^2 + 4(R^{r\phi}{}_{r\phi})^2 + 4(R^{\theta\phi}{}_{\theta\phi})^2. \tag{35}$$

That imposing the spherical symmetry conditions can be written in a reduced form by the expression below:

$$K = 4(R^{tr}{}_{tr})^2 + 8(R^{t\theta}{}_{t\theta})^2 + 8(R^{r\theta}{}_{r\theta})^2 + 4(R^{\theta\phi}{}_{\theta\phi})^2. \tag{36}$$

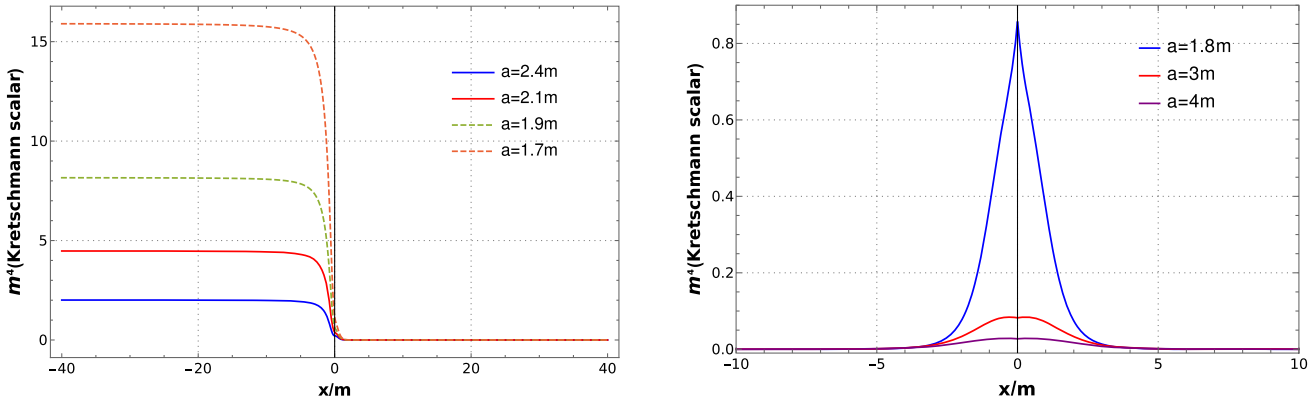

FIG. 6. The figure plots on the right represent the Kretschmann scalar for selected throat parameter values m, with $a = 1.8m$ inside the horizon (blue curve) and $a = 3m$, $4m$ outside the horizon (red and purple curves, respectively). On the left, we have the Kretschmann scalar for some throat values inside and outside the horizon for the general expression Eq. (17).

The Riemann tensor components in Eq. (34) show the Kretschmann scalar must be defined piecewise due to its dependence on the metric function $A_{\pm}(x)$. Thus, the Kretschmann scalar is

$$K_{+}(x) = \frac{(\Sigma^2 A_{+}'')^2 + 2(\Sigma\Sigma' A_{+}')^2 + 2\Sigma^2(\Sigma' A_{+}' + 2A_{+}\Sigma'')^2 + 4(1 - A_{+}\Sigma'^2)^2}{\Sigma^4}, \qquad x \geq 0,$$
$$K_{-}(x) = \frac{(\Sigma^2 A_{-}'')^2 + 2(\Sigma\Sigma' A_{-}')^2 + 2\Sigma^2(\Sigma' A_{-}' + 2A_{-}\Sigma'')^2 + 4(1 - A_{-}\Sigma'^2)^2}{\Sigma^4}, \qquad x \leq 0, \tag{37}$$

$$K(x \to 0) = \frac{4(3a^2 - 8am + 12m^2)}{a^6}. \tag{38}$$

Note that in Eq. (38), the Kretschmann scalar is regular in the limit of $x \to 0$, and therefore, no singularity is present. Likewise, in the limit of $x \to \pm\infty$, the scalar goes to zero.

Figure 6(b) plots the Kretschmann scalar for throat radii inside and outside the horizon. For $a = 1.8m$ within the horizon, Eq. (38) demonstrates a finite value at the origin. Similarly, the curves for radii outside the horizon also exhibit finite values at the origin.

A. Energy conditions

Analyzing the null energy conditions requires starting from Einstein's equations [45], previously defined in Eq. (2). This gives the nonzero stress-energy tensor components [46] as

$$T^{\mu}{}_{\nu} = \mathrm{diag}[\rho^{\phi}, -p_1^{\phi}, -p_2^{\phi}, -p_2^{\phi}], \tag{39}$$

where ρ^{ϕ} is the scalar field energy density, p_1^{ϕ} the radial pressure, and p_2^{ϕ} the tangential pressure. Using the stress-energy tensor diagonal component expressions in Eqs. (5) and (6) for the k-essence configuration $n = \frac{1}{3}$ from Eq. (24) and associated potential equation (28),

$$\rho_{\pm}^{\phi} = -\frac{F_0}{2}[-\eta A_{\pm}(\phi_{\pm}')^2]^{\frac{1}{3}} + V_{\pm}(x) = -\frac{3A_{\pm}\Sigma''}{\Sigma} + V_{\pm}(x), \tag{40}$$

$$p_{1\pm}^{\phi} = -T_1^1 = \frac{A_{\pm}\Sigma''}{\Sigma} - V_{\pm}(x), \tag{41}$$

$$p_{2\pm}^{\phi} = -T_2^2 = -T_0^0 = -\rho_{\pm}^{\phi} = \frac{3A_{\pm}\Sigma''}{\Sigma} - V_{\pm}(x). \tag{42}$$

The defined stress-energy tensor diagonal components are only valid outside the horizon where $A_{\pm} > 0$, with metric signature $(+,-,-,-)$ and t timelike and x spacelike.

Inside the horizon, t becomes spacelike and x timelike. The signature changes to $(-,+,-,-)$ with $A_{\pm} < 0$, reversing the coordinate roles. The stress-energy tensor components must then be rewritten as

$$T^{\mu}{}_{\nu} = \mathrm{diag}[-p_1^{\phi}, \rho^{\phi}, -p_2^{\phi}, -p_2^{\phi}], \tag{43}$$

and therefore, the equations for energy density, radial pressure, and tangential pressure must be rewritten as

$$\rho^{\phi}_{\pm} = -\frac{A_{\pm}\Sigma''}{\Sigma} + V_{\pm}(x), \tag{44}$$

$$p^{\phi}_{1\pm} = \frac{3A_{\pm}\Sigma''}{\Sigma} - V_{\pm}(x), \tag{45}$$

$$p^{\phi}_{2\pm} = -T^2_2 = -T^0_0 = -\rho^{\phi}_{\pm} = -(-p^{\phi}_{1\pm}) = \frac{3A_{\pm}\Sigma''}{\Sigma} - V_{\pm}(x). \tag{46}$$

The constructed geometric quantities depend on the metric function $A_{\pm}(x)$, so they are defined piecewise. With the defined energy density and pressure components, the energy conditions for black-bounce solutions can now be examined [39].

The commonly used energy conditions are inequalities relating the energy density and pressures [39]:

$$\mathrm{NEC}_{1,2} = \mathrm{WEC}_{1,2} = \mathrm{SEC}_{1,2} \Longleftrightarrow \rho^{\phi}_{\pm} + p^{\phi}_{(1,2)\pm} \geq 0, \tag{47}$$

$$\mathrm{SEC}_3 \Longleftrightarrow \rho^{\phi}_{\pm} + p^{\phi}_{1\pm} + 2p^{\phi}_{2\pm} \geq 0, \tag{48}$$

$$\mathrm{DEC}_{1,2} \Longleftrightarrow \rho^{\phi}_{\pm} + p^{\phi}_{(1,2)\pm} \geq 0 \quad \text{and} \quad \rho^{\phi}_{\pm} - p^{\phi}_{(1,2)\pm} \geq 0, \tag{49}$$

$$\mathrm{DEC}_3 = \mathrm{WEC}_3 \Longleftrightarrow \rho^{\phi}_{\pm} \geq 0. \tag{50}$$

The energy conditions can be explicitly expressed in terms of the metric functions by substituting the stress-energy tensor components from Eqs. (40)–(42) into the defining inequalities Eqs. (47)–(50).

This gives the energy conditions in the timelike region outside the event horizon where $A_{\pm} > 0$ as

$$\mathrm{NEC}^{\phi}_1 = \mathrm{WEC}^{\phi}_1 = \mathrm{SEC}^{\phi}_1 \Longleftrightarrow -\frac{2A_{\pm}\Sigma''}{\Sigma} \geq 0, \tag{51}$$

$$\mathrm{NEC}^{\phi}_2 = \mathrm{WEC}^{\phi}_2 = \mathrm{SEC}^{\phi}_2 \Longleftrightarrow 0, \tag{52}$$

$$\mathrm{SEC}^{\phi}_3 \Longleftrightarrow \frac{4\Sigma''A_{\pm}}{\Sigma} - 2V_{\pm}(x) \geq 0, \tag{53}$$

$$\mathrm{DEC}^{\phi}_1 \Longleftrightarrow -\frac{4\Sigma''A_{\pm}}{\Sigma} + 2V_{\pm}(x) \geq 0, \tag{54}$$

$$\mathrm{DEC}^{\phi}_2 \Longleftrightarrow -\frac{6\Sigma''A_{\pm}}{\Sigma} + 2V_{\pm}(x) \geq 0, \tag{55}$$

$$\mathrm{DEC}^{\phi}_3 = \mathrm{WEC}^{\phi}_3 \Longleftrightarrow -\frac{3A_{\pm}\Sigma''}{\Sigma} + V_{\pm}(x) \geq 0. \tag{56}$$

Likewise, the energy conditions inside the horizon where t is spacelike are obtained by substituting the stress-energy tensor components from Eqs. (44)–(46) into the inequalities Eqs. (47)–(50). This gives the energy conditions for $A_{\pm} < 0$ as

$$\mathrm{NEC}^{\phi}_1 = \mathrm{WEC}^{\phi}_1 = \mathrm{SEC}^{\phi}_1 \Longleftrightarrow \frac{2A_{\pm}\Sigma''}{\Sigma} \geq 0, \tag{57}$$

$$\mathrm{NEC}^{\phi}_2 = \mathrm{WEC}^{\phi}_2 = \mathrm{SEC}^{\phi}_2 \Longleftrightarrow \frac{2A_{\pm}\Sigma''}{\Sigma} \geq 0, \tag{58}$$

$$\mathrm{SEC}^{\phi}_3 \Longleftrightarrow \frac{8A_{\pm}\Sigma''}{\Sigma} - 2V_{\pm}(x) \geq 0, \tag{59}$$

$$\mathrm{DEC}^{\phi}_1 \Longleftrightarrow -\frac{4A_{\pm}\Sigma''}{\Sigma} + 2V_{\pm}(x) \geq 0, \tag{60}$$

$$\mathrm{DEC}^{\phi}_2 \Longleftrightarrow -\frac{4A_{\pm}\Sigma''}{\Sigma} + 2V_{\pm}(x) \geq 0, \tag{61}$$

$$\mathrm{DEC}^{\phi}_3 = \mathrm{WEC}^{\phi}_3 \Longleftrightarrow -\frac{A_{\pm}\Sigma''}{\Sigma} + V_{\pm}(x) \geq 0. \tag{62}$$

Equations (51) and (57) demonstrate that the null energy condition (NEC^{ϕ}_1) is violated both inside and outside the event horizon. Likewise, NEC^{ϕ}_2 given by Eq. (52) is satisfied outside the horizon but violated inside according

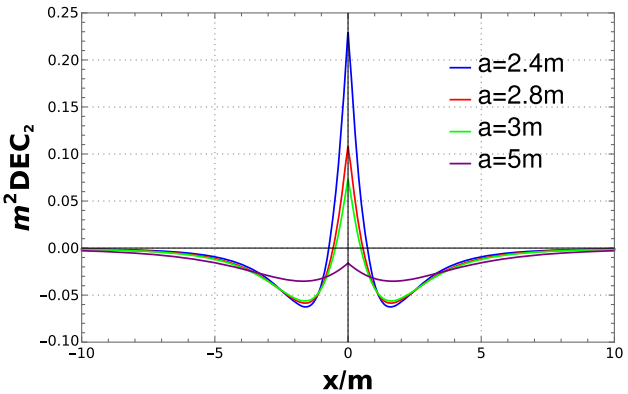

(a)

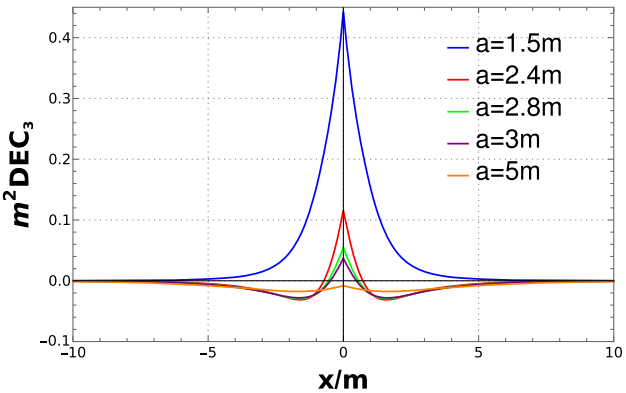

(b)

FIG. 7. DEC plot relating energy density and tangential pressure, for radii inside and outside the event horizon.

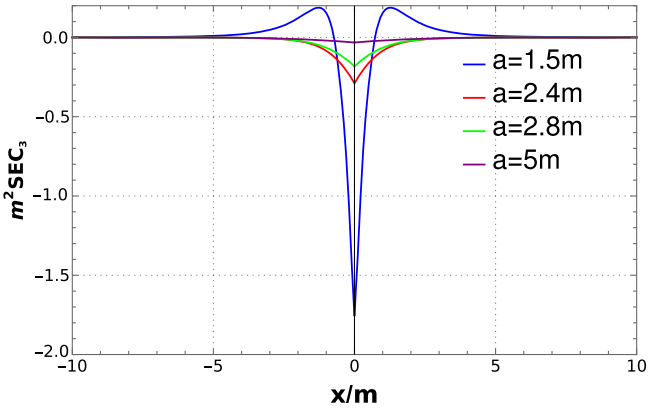

FIG. 8. Strong energy condition (SEC) plot combining energy density and all pressure components, for various radii inside and outside the horizon.

to Eq. (58). Since DEC_2^{ϕ} is connected to NEC_2^{ϕ}, it is also violated within the horizon through Eq. (61). Similarly, DEC_1^{ϕ} is violated both outside and inside the horizon, which is tied to the violation of (NEC_1^{ϕ}).

Complementarily, Fig. 7(a) exhibits DEC_2^{ϕ} violation for all radii outside the horizon. However, DEC_3^{ϕ} violates outside but satisfies inside the horizon [Fig. 7(b)]. Finally, SEC_3^{ϕ} violates inside and outside, as shown in Fig. 8.

V. CONCLUSION

The present analysis utilizes the k-essence field equations describing a phantom scalar field to construct black-bounce solutions not possible with an ordinary scalar field. It should be noted that k-essence does not constitute a modified theory of gravity; rather, it introduces a scalar field through a nonstandard kinetic term. The analysis begins with the areal metric function $\Sigma^2 = x^2 + a^2$ containing a throat radius a as in the original black-bounce proposals [1]. The corresponding metric function in k-essence theory is derived by applying boundary conditions to obtain an asymptotically flat spacetime. This defines the full metric and enables study of the black-bounce structures.

The analysis attempts to satisfy the equations of motion with only a kinetic term for the scalar field. However, this is insufficient, requiring introduction of a scalar potential as well. Analytical expressions for the scalar field and necessary potential are derived, with the full set of equations satisfied. The possibility of using alternative black-bounce throat metric functions, as studied in Ref. [3], is also examined but leads to algebraically intractable solutions.

With the derived analytical metric function and known black-bounce throat function, the Kretschmann scalar is verified to be regular at the origin for radii inside and outside the horizon. The mixed stress-energy tensor components are defined on each side of the horizon, with the roles of t and x reversed. Analysis of the energy conditions shows violation of the null energy condition (NEC_1^{ϕ}) inside and outside the horizon, consistent with other black-bounce solutions. Violation of the null energy condition is the main ingredient for building regular black-bounce geometries.

As is well known, in general relativity the strong energy condition (SEC_3) is typically violated within the event horizon for regular black hole solutions, while the weak energy condition (WEC) can be violated throughout spacetime in some cases [1,4]. However, the solution presented in this work exhibits different behavior, with the strong energy condition (SEC_3^{ϕ}) being violated both outside and inside the event horizon, as shown in Fig. 8. Meanwhile, the weak energy condition (WEC_3^{ϕ}) is violated outside the horizon but satisfied inside, as depicted in Fig. 7(b).

An interesting observation is that due to the visual form that the potential takes in Fig. 5 we may be indicating a possible stability of the solutions when subjected to radial perturbations, considering the possibility of having normal and quasinormal modes [40–43].

ACKNOWLEDGMENTS

We thank CNPq, CAPES, and FAPES for financial support. The authors thank M. V. S. Silva and E. L. Martins for their fruitful discussions.

APPENDIX: THIN SHELL IN BACK-BOUNCE SOLUTION

This section is reserved to demonstrate the sign of the mass of the surface at the point where the metric function was matched [Eq. (23)]. For the line element contained in Eq. (33), the following coordinate transformation will be considered: $r^2 = x^2 + a^2$ which transforms into an equivalent line element and was adopted in [47,48,49]. It is emphasized that in this last section, the same signature of the metric will be used as in the cited works above so that the results can be better compared. In this way, the line element Eq. (33) gets rewritten as

$$ds^2 = A_{\pm}(r)dt^2 - \frac{dr^2}{A_{\pm}(r)(1-\frac{a^2}{r^2})} - r^2 d\Omega^2. \quad \text{(A1)}$$

The metric function $A_{\pm}(r)$ is defined in terms of the new coordinate as

$$A_{\pm}(r) = 1 \pm \frac{4m}{\pi a^3}\left[a(\sqrt{r^2-a^2}) + r^2\left(\arctan\left(\frac{\sqrt{r^2-a^2}}{a}\right) \mp \frac{\pi}{2}\right)\right]. \quad \text{(A2)}$$

In the original metric [Eq. (33)], the coordinates x and t are defined over the entire space $x \in (-\infty, +\infty)$ and $t \in (-\infty, +\infty)$ [1]. In the new coordinates [Eq. (A1)], the temporal part t retains the same range, but the radial part

domain is modified to $r \in (a, +\infty)$. The line element describing the thin shell is given by

$$ds^2 = d\tau^2 - R^2(\tau) d\Omega^2, \tag{A3}$$

where the parameter τ corresponds to the proper time for an observer in the shell.

To compute the extrinsic curvature, the 4-velocity vector $U^\mu = (\frac{dt}{d\tau}, \frac{dR(\tau)}{d\tau}, 0, 0)$ and normal vector n^μ to the hypersurface are first defined. The 4-velocity vector can be expressed in terms of the metric components in Eq. (A1) as

$$U^\mu_\pm = \pm\left[\sqrt{\frac{(1 + g_{11}\dot{R}^2)}{g_{00}}}, \dot{R}, 0, 0\right], \tag{A4}$$

on what $\dot{R} = \frac{dR}{d\tau}$ and $U\mu U^\mu = 1$.

In the same way, we will define the normal vector to the surface. For this, we will need to perform a parametrization in terms of the intrinsic coordinates $\xi^i = (\tau, \theta, \phi)$, Eq. (A3). Therefore, the parametrization is defined as $f(x^\mu(\xi^i)) = r - R(\tau) = 0$, and the normal unit 4-vector is given by the expression

$$n_\mu = \frac{\nabla_\mu f}{\|\nabla f\|} = \pm\left| g^{\alpha\beta} \frac{\partial f}{\partial x^\alpha} \frac{\partial f}{\partial x^\beta} \right|^{-\frac{1}{2}} \frac{\partial f}{\partial x^\mu}. \tag{A5}$$

The normal vector is unitary $n_\mu n^\mu = -1$ and orthogonal to the vectors tangent to the surface $n_\mu e^\mu_i = n_\mu(\frac{\partial x^\mu}{\partial \xi^i}) = 0$. Therefore, the normal vector written in terms of the components of the metric Eq. (A1) is given by

$$n^\mu_\pm = \pm\left[\dot{R}\sqrt{-\frac{g_{11}}{g_{00}}}, \sqrt{-g^{11} + \dot{R}^2}, 0, 0\right]. \tag{A6}$$

With the constructed normal vector n^μ and 4-velocity vector U^μ, the extrinsic curvature can be defined as

$$K^\pm_{ij} = -n_\mu\left[\frac{\partial^2 x^\mu}{\partial\xi^i \partial\xi^j} + \Gamma^{\mu\pm}_{\alpha\beta} \frac{\partial x^\alpha}{\partial \xi^i} \frac{\partial x^\beta}{\partial \xi^j}\right]. \tag{A7}$$

The $\theta\theta$ component of the extrinsic curvature is computed, as it is related to the surface energy density. Thus, its explicit form is given by

$$K^{\theta\pm}_\theta = \pm\frac{1}{R}\left[A_\pm\left(1 - \frac{a^2}{R^2}\right) + \dot{R}^2\right]^{\frac{1}{2}}. \tag{A8}$$

1. Lanczos equation

The discontinuity across the thin shell is characterized by the difference in extrinsic curvature outside and inside, $k_{ij} = K^+{}_{ij} - K^-{}_{ij}$. The Einstein equation in the interior spacetime yields the Lanczos equation:

$$S^i_j = -\frac{1}{8\pi}(k^i_j - \delta^i_j k^k_k), \tag{A9}$$

where S^i_j are the nonzero components of the surface stress-energy tensor, $S^i_j = \mathrm{diag}(-\sigma, \mathcal{P}, \mathcal{P})$. Here, σ is the surface energy density and $\mathcal{P}$ is the pressure. The $\tau\tau$ component of the Lanczos equation yields the surface energy density:

$$\sigma = -\frac{1}{4\pi}k^\theta_\theta = -\frac{1}{2\pi R}\left[A_\pm\left(1 - \frac{a^2}{R^2}\right) + \dot{R}^2\right]^{\frac{1}{2}}. \tag{A10}$$

At the junction point $x = 0$, the metric function takes the Simpson-Visser form $A_\pm = (1 - \frac{2m}{R})$ [1]. For a static shell with $\dot{R} = 0$, the energy density in Eq. (A10) becomes

$$\sigma = -\frac{1}{2\pi R}\left[\left(1 - \frac{2m}{R}\right)\left(1 - \frac{a^2}{R^2}\right)\right]^{\frac{1}{2}}. \tag{A11}$$

Therefore, by analyzing the expression for the static energy density in Eq. (A11), we see that the product of the terms inside the square root imposes two constraints to be positive: $R > a$ and whether the shell is inside or outside the event horizon. Note that for any shell value greater than the throat radius a, the second term inside the square root is always positive. However, the first term inside the square root depends on whether the shell is inside $A_\pm < 0$ or outside $A_\pm > 0$ the event horizon. This implies that black-bounce solutions are possible only for two-way traversable wormholes with $a > 2m$ and wormholes with symmetric horizons $a < 2m$.

The static energy density in Eq. (A11) can be analyzed generally, without requiring evaluation specifically at the junction surface. Notably, the metric function in Eq. (A2) is positive for throat radii outside the horizon, $a > 2m$, and negative inside, $a < 2m$ [Fig. 1(b)]. The surface mass is defined as $m_s = 4\pi R^2\sigma$. Therefore, for solutions with $a > 2m$, the surface density σ is negative, aligning with the violation of energy conditions observed in Fig. 7(b). Conversely, for solutions with $a < 2m$, the surface density σ is positive, representing no violation of energy conditions as seen in Fig. 7(b).

[1] A. Simpson and M. Visser, J. Cosmol. Astropart. Phys. 02 (2019) 042.
[2] F. S. N. Lobo, M. E. Rodrigues, M. V. d. S. Silva, A. Simpson, and M. Visser, Phys. Rev. D **103**, 084052 (2021).
[3] M. E. Rodrigues and M. V. d. S. Silva, Classical Quantum Gravity **40**, 225011 (2023).
[4] E. L. B. Junior and M. E. Rodrigues, Gen. Relativ. Gravit. **55**, 8 (2023).
[5] K. A. Bronnikov and J. C. Fabris, Phys. Rev. Lett. **96**, 251101 (2006).
[6] C. Armendariz-Picon, V. Mukhanov, and P. J. Steinhardt, Phys. Rev. D **63**, 103510 (2001).
[7] C. Armendariz-Picon, T. Damour, and V. Mukhanov, Phys. Lett. B **458**, 209 (1999).
[8] C. Armendariz-Picon, V. Mukhanov, and P. J. Steinhardt, Phys. Rev. Lett. **85**, 4438 (2000).
[9] R. Leigh, Mod. Phys. Lett. A **04**, 2767 (1989).
[10] K. A. Bronnikov, Phys. Rev. D **106**, 064029 (2022).
[11] K. A. Bronnikov and R. K. Walia, Phys. Rev. D **105**, 044039 (2022).
[12] P. Cañate, Phys. Rev. D **106**, 024031 (2022).
[13] P. Cañate and F. H. Maldonado-Villamizar, Phys. Rev. D **106**, 044063 (2022).
[14] M. E. Rodrigues and M. V. de S. Silva, Phys. Rev. D **107**, 044064 (2023).
[15] E. Franzin, S. Liberati, J. Mazza, A. Simpson, and M. Visser, J. Cosmol. Astropart. Phys. 07 (2021) 036.
[16] J. Mazza, E. Franzin, and S. Liberati, J. Cosmol. Astropart. Phys. 04 (2021) 082.
[17] A. Simpson, P. Martin-Moruno, and M. Visser, Classical Quantum Gravity **36**, 145007 (2019).
[18] K. A. Bronnikov, V. A. G. Barcellos, L. P. de Carvalho, and J. C. Fabris, Eur. Phys. J. C **81**, 395 (2021).
[19] J. R. Nascimento, A. Y. Petrov, P. J. Porfirio, and A. R. Soares, Phys. Rev. D **102**, 044021 (2020).
[20] Naoki Tsukamoto, Phys. Rev. D **104**, 064022 (2021).
[21] Naoki Tsukamoto, Phys. Rev. D **103**, 024033 (2021).
[22] Naoki Tsukamoto, Phys. Rev. D **105**, 084036 (2022).
[23] S. Ghosh and A. Bhattacharyya, J. Cosmol. Astropart. Phys. 11 (2022) 006.
[24] A. Chowdhuri, S. Ghosh, and A. Bhattacharyya, Front. Phys. **11**, 164 (2023).
[25] H. Aounallah, A. R. Soares, and R. L. L. Vitoria, Eur. Phys. J. C **80**, 447 (2020).
[26] A. R. Soares, R. L. L. Vitoria, and H. Aounallah, Eur. Phys. J. Plus **136**, 966 (2021).
[27] C. F. S. Pereira, A. R. Soares, R. L. L. Vitoria, and H. Belich, Eur. Phys. J. C **83**, 270 (2023).
[28] A. Moussa, H. Aounallah, P. Rudra, and F. Ahmed, Int. J. Geom. Methods Mod. Phys. **20**, 2350102 (2023).
[29] F. S. N. Lobo, Phys. Rev. D **71**, 084011 (2005).
[30] M. S. Churilova, R. A. Konoplya, Z. Stuchlik, and A. Zhidenko, J. Cosmol. Astropart. Phys. 10 (2021) 010.
[31] K. A. Bronnikov, R. A. Konoplya, and A. Zhidenko, Phys. Rev. D **86**, 024028 (2012).
[32] Alberto Rozas-Fernández, Phys. Lett. B **709**, 23 (2012).
[33] Mustafa Salti, Eur. Phys. J. Plus **129**, 42 (2014).
[34] C. J. Gao and S. N. Zhang, arXiv:hep-th/0604114.
[35] M. Azreg-Ainou, G. Clement, J. C. Fabris, and M. E. Rodrigues, Phys. Rev. D **83**, 124001 (2011).
[36] E. F. Eiroa and C. M. Sendra, Phys. Rev. D **88**, 103007 (2013).
[37] Y. Huang, S. Chen, and J. Jing, Eur. Phys. J. C **76**, 594 (2016).
[38] K. A. Bronnikov, J. C. Fabris, and D. C. Rodrigues, Gravitation Cosmol. **22**, 26 (2016).
[39] M. Visser, *Lorentzian Wormholes: From Einstein to Hawking* (AIP Press, New York, 1995).
[40] U. C. da Silva, C. F. S. Pereira, and A. A. Lima, Ann. Phys. (Amsterdam) **460**, 169549 (2024).
[41] J. C. Fabris, M. G. Richarte, and A. Saa, Phys. Rev. D **103**, 045001 (2021).
[42] D. P. Du, B. Wang, and R. K. Su, Phys. Rev. D **70**, 064024 (2004).
[43] Y. Zhong, J. High Energy Phys. 09 (2022) 165.
[44] K. A. Bronnikov and S. G. Rubin, *Black Holes, Cosmology and Extra Dimensions* (World Scientific, Singapore, 2013).
[45] R. M. Wald, *General Relativity* (The University of Chicago Press, Chicago, 1984).
[46] R. D'Inverno, *Introducing Einstein's Relativity* (Oxford University Press, New York, 1998).
[47] A. Simpson, arXiv:2304.07383.
[48] F. S. N. Lobo, A. Simpson, and M. Visser, Phys. Rev. D **101**, 124035 (2020).
[49] N. M. Garcia, F. S. N. Lobo, and M. Visser, Phys. Rev. D **86**, 044026 (2012).